RESEARCH ARTICLE

PROGRESS IN
PHOTOVOLTAICS WILEY

Interdigitated back-contacted structure: A different approach towards high-efficiency ultrathin copper indium gallium (di) selenide solar cells

Nasim Rezaei[1] | Paul Procel[1] | Marcel Simor[2] | Zeger Vroon[3] |
Miro Zeman[1] | Olindo Isabella[1]

[1]PVMD Lab., Delft University of Technology, Mekelweg 4, Delft, 2628 CD, The Netherlands

[2]Solar Technology and Application, TNO/Solliance, High Tech Campus 21, Eindhoven, 5656 EA, The Netherlands

[3]TNO-Brightlands Materials Center, TNO, Urmondsebaan 22, 6167 RD Geleen, PO BOX 18, Geleen, 6160 MD, The Netherlands

Correspondence
Nasim Rezaei, PVMD Lab., Delft University of Technology, Mekelweg 4, 2628 CD Delft, The Netherlands.
Email: n.rezaei@tudelft.nl

Abstract

An interdigitated back-contacted (IBC) configuration is proposed for submicron copper indium gallium (di)selenide (CIGS). In a modelling platform, the structure was opto-electrically optimized for maximum efficiency. The results are compared with a reference front/back-contacted (FBC) solar cell with similar absorber thickness and exhibiting 11.9% efficiency. The electrical passivation at the front side is accomplished by an Al_2O_3 layer, which is endowed with negative fixed charges. The results indicate that with an optimal geometry and engineered bandgap grading, the efficiency of the new IBC structure can reach 17%. Additionally, with a reasonably low defect density in the absorber layer, efficiencies as high as 19.7% and open-circuit voltage comparable with that of the record solar cell are possible with the IBC structure.

KEYWORDS

bandgap grading, CIGS solar cells, electrical modelling, IBC, light management

1 | INTRODUCTION

High absorption coefficient and tuneable bandgap (between 1 and 1.7 eV) make copper indium gallium (di)selenide (CIGS) an appropriate absorber material for highly efficient thin-film solar cell applications.[1–3] Yet, with a world record efficiency of 23.35%,[4,5] CIGS solar cells are still far from the Shockley–Queisser (SQ) theoretical efficiency limit.[6,7] This gap is even wider for submicron CIGS solar cells, which for various reasons are studied by different research groups.[8–10] In addition to optical losses, submicron CIGS solar cells suffer from other performance deteriorations, which generally lead to less than optimal efficiencies.[11] In this respect, different strategies such as light management,[12–14] back contact passivation[8,15,16] and alternative front layers[5,17] have been employed to increase the performance of both thick (>1 μm) and ultrathin CIGS solar cells.

However, in the front/back-contacted (FBC) structure, there are inevitable optical losses due to the parasitic absorption of the top layers, accounting for more than 10% loss in photocurrent density (J_{ph}).[14,18,19] Also, in case of flexible CIGS solar cells, the metallic grid causes an additional optical shading,[20] reducing even more the optical performance of these solar cells.

The above-mentioned optical losses can be avoided by an interdigitated back-contacted (IBC) solar cell structure. In IBC structure, the electron-contact and hole-contact (e-contact and h-contact, respectively) are both located at the rear side of the absorber material in a periodic design.[21–33] In our previous work,[27] we investigated the optical performance potential of a novel IBC CIGS solar cell with and without textured antireflection coating (ARC). In this work, we employ opto-electrical simulations in TCAD Sentaurus environment to further study and optimize an IBC CIGS

TABLE 1 The model parameters used in TCAD simulations

Layer parameter	Symbol (unit)	CIGS[19,35]	CdS[35]	CIGS/CdS[35]	i-ZnO[35]	AZO[35]	GZO-a[36]
Thickness	d (nm)	673	50		50	205	330
Bandgap FBC/IBC	E_g(eV)	Graded	2.4		3.3	3.3	3.25
Electron affinity FBC/IBC	χ (eV)	Graded	4.2		4.3	4.3	**4.3**
Rel. permittivity	ε_r	13.6	5.4		9	9	3.85
Doping	N_A, N_D (cm^{-3})	2×10^{16} (A)	5×10^{17} (D)		1×10^{17} (D)	1×10^{20} (D)	3.2×10^{19} (D)
CB DOS	N_C (cm^{-3})	6.8×10^{17}	1.3×10^{18}		3×10^{18}	3×10^{18}	3.7×10^{18}
VB DOS	N_V (cm^{-3})	1.5×10^{19}	9.1×10^{19}		1.7×10^{19}	1.7×10^{19}	$\mathbf{1.7 \times 10^{19}}$
Mobility	μ_e, μ_h (cm^2 V^{-1} s^{-1})	100, 12.5	72, 20		100, 31	100, 31	23.1, 7
Defects							
Type	–	D	A	D	A	A	A
Concentration/density	N_T (cm^{-3})/N_{IF} (cm^{-2})	5×10^{13}	2×10^{17}	1×10^{12}	1×10^{16}	1×10^{16}	$\mathbf{1 \times 10^{16}}$
Energy level	E_T	E_i	E_i	E_i	E_i	E_i	$\boldsymbol{E_i}$
Cap. cross-sec.	σ_e, σ_h (cm^2)	5×10^{-13}, 1×10^{-15}	1×10^{-15}, 5×10^{-13}	5×10^{-13}, 1×10^{-15}	1×10^{-15}, 5×10^{-13}	1×10^{-15}, 5×10^{-13}	$\mathbf{1 \times 10^{-15}}$, $\mathbf{5 \times 10^{-13}}$

Note: A and D denote acceptor and donor, respectively. CB DOS and VB DOS represent density of states of conduction band minimum and valance band maximum, respectively. Subscript IF means interface. The parameters and values shown in bold are fitting parameters. CIGS/CdS column reports input data referring to the interface between CIGS and CdS layers.

solar cell. First, we calibrate the model by matching the current density versus voltage (J-V) curves of simulated FBC CIGS solar cells with experimentally measured curves. Then, after explaining the IBC design strategy, we optimize geometrical and material properties in a step-by-step approach, keeping both efficiency and practicability in mind.

2 | MODELLING APPROACH

We used a two-dimensional (2-D) simulation approach for both the FBC and IBC solar cell structures in TCAD Sentaurus environment. This simulation tool solves drift–diffusion equations by considering the thickness of the layers, trap distributions, doping, band structures and layers' optical properties.[34] We modelled opto-electrically the layered structures and selected the transfer matrix method (TMM) for the optical modelling. Using the reference FBC cells fabricated in Solliance Solar Research institute, we performed atomic force microscopy (AFM) to measure the root mean square (RMS) roughness in two cases: (i) the ZnO:Al (AZO) surface of the full solar cells and (ii) the bare CIGS surface after removing the front contact layers. The average RMS roughness of several samples was between 30 and 45 nm for AZO and CIGS surfaces, respectively. We used these values in the optical model to take into consideration the light scattering from the normally incident AM1.5G spectrum at rough interfaces. The model parameters used in this work are summarized in Table 1. In these simulations, we have modelled the natural defects in the CIGS material with donor-type midgap recombination centres.[35] Note that our primary goal is not to model the exact complicated nature of the CIGS material. We rather replicated the cell's performance by using an equivalent recombination behaviour.[35]

In our simulation framework, the mesh elements are forced to be smaller near interfaces to accurately account for interface recombination and charge transport. In case of CIGS with Ga grading, the change in the Ga content affects the wavelength-dependent optical constants—refractive index, $n(\lambda)$, and extinction coefficient, $k(\lambda)$—and, hence, the bandgap and absorption coefficient. In this work, we use an energy-shift model[37] to calculate the optical constants of CIGS with an arbitrary Ga composition. In this respect, multiple sets of $n(\lambda)$ and $k(\lambda)$ with known Ga compositions[1,19] were employed, from which the optical constants of intermediate arbitrary Ga contents were calculated. The optical constants of other materials were obtained from previous studies.[36,38–42]

3 | MODEL CALIBRATION

We calibrated our simulations by comparing the J-V curves of the simulated FBC solar cells with those of the fabricated cells from Solliance Solar Research institute. From the light-facing side, the reference cell structure consists of AZO, intrinsic ZnO (i-ZnO), CdS, CIGS and Mo (Figure 1A). A close match between the simulated
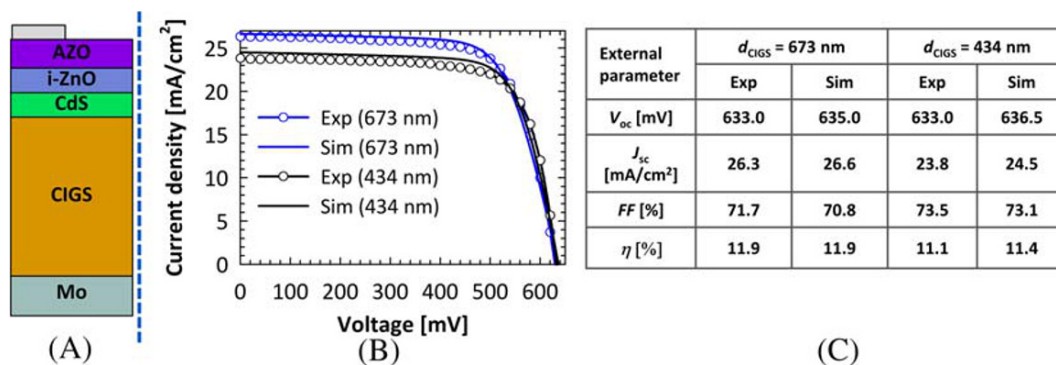
FIGURE 1 A, The reference front/back-contacted (FBC) solar cell as modelled by TCAD (dimensions are not to scale). The dashed line shows the symmetry plane. B, *J-V* curves of the simulated and fabricated solar cells. The numbers in brackets indicate the absorber thickness. C, The measured and simulated external parameters of the reference FBC solar cell for two different absorber thicknesses [Colour figure can be viewed at wileyonlinelibrary.com]

and measured external parameters—short-circuit current density (J_{SC}), open-circuit voltage (V_{OC}), fill factor (*FF*) and efficiency (η)—for different absorber thicknesses indicates the validity of the model (Figure 1B,C). The fitting has been achieved by mostly adjusting the thickness of different layers, including the absorber layer. The variable absorber bandgap is included in the calibration models. Due to different deposition parameters for varying absorber thickness, the bandgap grading is different and sample-dependent. For instance, the 443-nm-thick CIGS model was fitted to the experimental data by a slight increase of the bandgap towards the CIGS/Mo interface (from 1.17 to 1.21 eV). This in case of the 673-nm-thick CIGS model was done by increasing the bandgap from 1.16 to 1.2 eV from the surface to the CIGS/Mo interface.

4 | IBC DESIGN CONSIDERATIONS

The not-in-scale schematic of the proposed IBC solar cell structure is shown in Figure 2A. In a more realistic scale, the CIGS thickness will be even smaller than the gap width (*Gap*). The absorber thickness is kept similar to that of the reference FBC solar cell (673 nm) for fair comparison. The model is mirror-like symmetric at half of the h-contact and periodic in *x* direction. In our previous work,[27] we optimized an Al_2O_3/MgF_2-based double-layer ARC for an IBC solar cell with natural surface morphology. The gradual change in the refractive index from MgF_2 to CIGS provides a wideband anti-reflection effect. The optimal thicknesses of Al_2O_3 and MgF_2 for this work are 80 and 85 nm, respectively. The Al_2O_3 layer at the front side of the absorber serves also as chemical and electrical
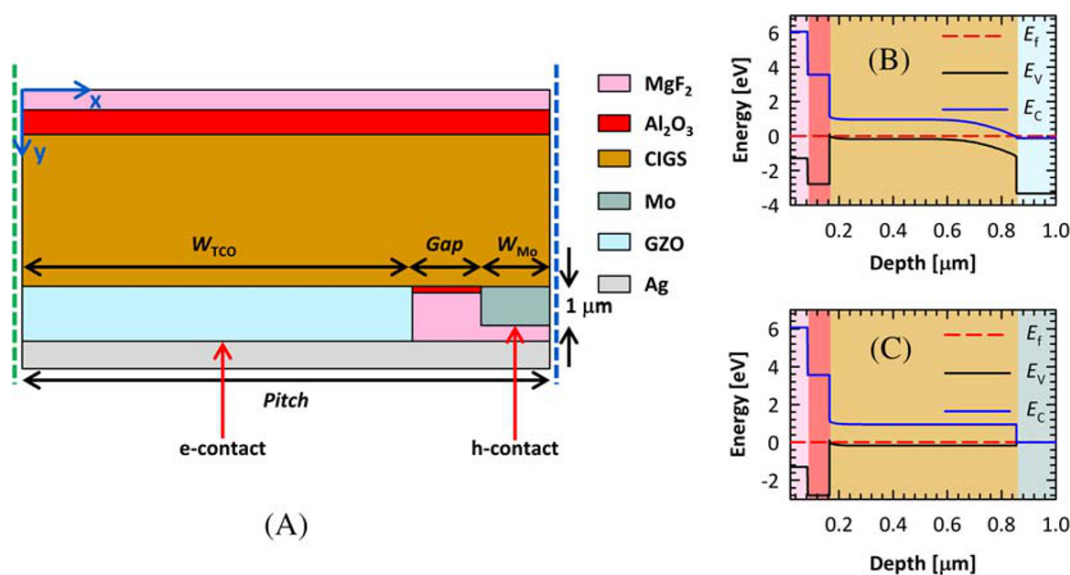
FIGURE 2 A, The schematic of the interdigitated back-contacted (IBC) solar cell (dimensions are not to scale) with symmetry (dashed blue) and periodicity (dashed green) lines. B,C, The band diagram of the e-contact and h-contact, respectively [Colour figure can be viewed at wileyonlinelibrary.com]

passivation layer. An annealing step at 400–450°C will activate negative fixed charges with densities as high as 1×10^{13} cm^{-2} at the CIGS/Al$_2$O$_3$ interface, leading to electrical passivation of the interface.[40,43] The presence of these fixed charges is considered in the model at the CIGS/Al$_2$O$_3$ interface both at the front and at the rear side of the absorber material. It is worth noting that the typical front layers in the FBC structure, that is, CdS, i-ZnO and AZO, are both not needed in and even detrimental to the IBC structure. This is because of parasitic absorption and the formation of a p-n junction at the front side of the absorber preventing the lateral transport of the charge carriers. Here, the impact of the absorber quality on absorption is of secondary importance. In fact, the comparison between our reference FBC solar cell and the proposed IBC design is merely related to the performance difference of the same absorber in two different configurations.

At the rear side, a silver reflector is placed to reflect the photons from the rear side for a second-absorption chance. At the experimental level, however, the IBC structure could be realized on other substrates.[27] The e- and h-contacts are separated by a dielectric stack consisting of MgF$_2$ and Al$_2$O$_3$ both to avoid electrical shunts and to increase the internal reflection due to the low refractive index of deployed dielectrics. The influence of the thin Al$_2$O$_3$ layer in electrical passivation will be studied in the following sections.

The e-contact is realized by an n-doped transparent conductive oxide (TCO). We intentionally did not use AZO for this purpose, because of its low thermal stability, which could become a problem at experimental level. In this case, gallium-doped zinc-oxide (GZO) *type-a* based on the work of Fujiwara and Kondo[36] was chosen. High doping concentration, low absorption coefficient, high thermal stability and low free carrier absorption are some of the advantages of such a GZO material over its counterparts.[36,44] Figure 2B shows the band diagram of the e-contact in dark condition. At the front side, the presence of negative fixed charges induces an electric field, which prevents the accumulation of electrons at the CIGS/Al$_2$O$_3$ interface (field effect passivation).[27,43] Also, the accumulation of holes at the front interface helps with the lateral transport of majority charge carriers towards the molybdenum contact (i.e., the h-contact). The band bending at the rear side shows the formation of a p-n junction between CIGS and the degenerate semiconductor, GZO, which functions well for electron collection and hole rejection.

Similar to the conventional FBC CIGS solar cells, the majority carriers are collected using a Mo contact. As also plotted in Figure 2C, the ohmic contact formed due to the formation of a very thin MoSe$_2$ layer at the CIGS/Mo interface enables the collection of holes.[27]

5 | RESULTS AND DISCUSSION

We have performed simulations by varying the geometrical parameters (Figure 2A) and absorber material characteristics to investigate the influence of each parameter on the cell performance. In each scenario, only one parameter is varied. After each step, the most suitable parameter value is selected for the rest of simulations to step-by-step complete the design of the proposed IBC structure. In-depth analysis of the charge density distribution or electric fields are provided when needed.

5.1 | TCO width

We started with varying the TCO width (W_{TCO}), while keeping *Gap* and the Mo width (W_{Mo}) constant. Since the gap region is a non-collecting region, its width should be as small as possible. Hence, in these models, *Gap* is chosen to be 1 μm. Nonetheless, a sensitivity study on *Gap* will be provided in the following sections. Also, W_{Mo} should be smaller than or comparable with the minority carrier diffusion length to facilitate low carrier recombination. Therefore, it is kept at 500 nm. Note that due to symmetry, in the complete structure, this value means that the total width of Mo is 1 μm. Also, a change in W_{TCO} leads to a change in the size of the simulation domain, *Pitch*. The external parameters as functions of the changes in W_{TCO} are plotted in Figure 3. We observe that V_{OC} and J_{SC} increase as W_{TCO} increases. This can be explained by the reduction of electrical shading, which refers to the local reduction of J_{SC} due to charge carrier recombination at regions other than e-contact.[45] On the other hand, wider e-contact means that the majority carriers need to travel in longer distances to be collected at the h-contact. This explains the reducing trend of *FF* in Figure 3, which slightly outbalances the increasing trend of V_{OC} and J_{SC} for W_{TCO} > 30 μm. For this reason and for the sake of
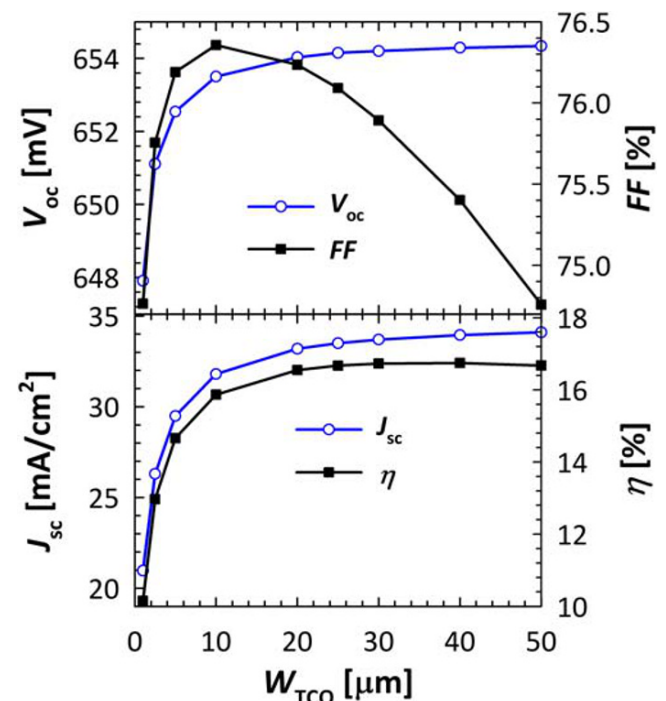
FIGURE 3 The external parameters as functions of W_{TCO}. The thickness of CIGS absorber layer is 673 nm [Colour figure can be viewed at wileyonlinelibrary.com]
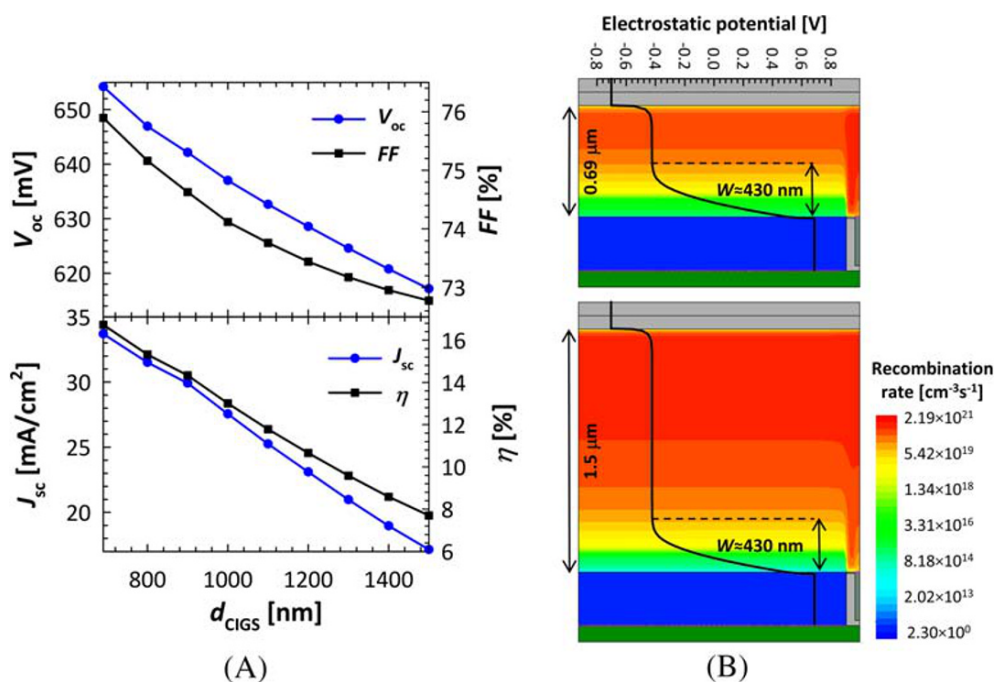
fast simulations, we chose W_{TCO} = 30 μm for the rest of our studies. Already for such a nonoptimized IBC architecture, the conversion efficiency is boosted to a value of 16.73%.
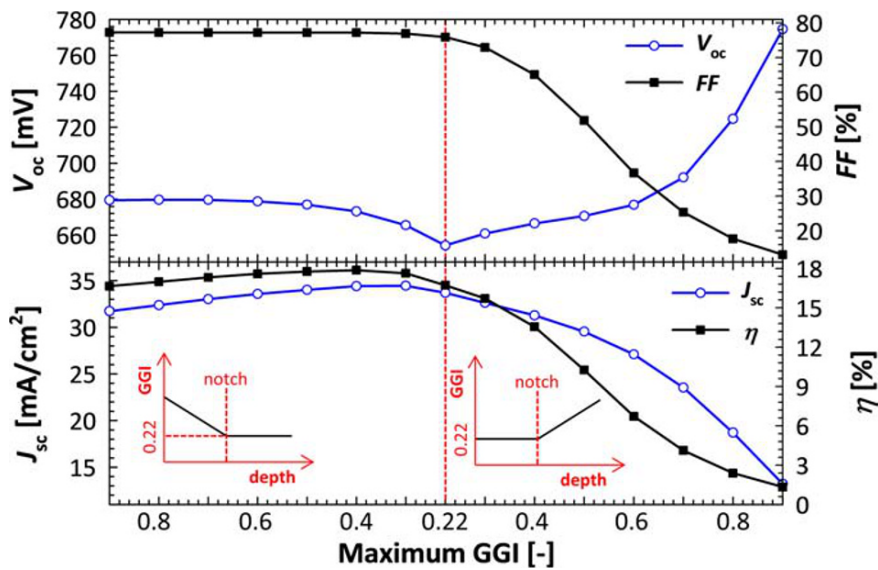
5.2 | Absorber thickness

We also studied the effect of the absorber thickness (d_{CIGS}) on the external parameters. We kept the bandgap constant at 1.16 eV and the rest of the geometrical parameters similar to the previous section. One would think that a thicker absorber naturally leads to higher current generation. However, as Figure 4A shows, the larger charge carrier generation (due to more light absorption) is debunked by more carrier recombination in the absorber bulk. The colour plot in Figure 4B shows the charge carrier recombination rate in short-circuit conditions for two absorber thicknesses, namely, 690 and 1500 nm. The significantly higher recombination in the CIGS bulk can be explained by the black curves overlaid on the solar cells' cross-section. The curves represent the electrostatic potential as a function of depth under equilibrium conditions, from which the extent of the depletion region in the absorber (W) can be calculated. Knowing that the electrostatic potential is constant outside the space charge region and varies inside the region, we calculated W for the above-mentioned thicknesses. Also, since the material properties, especially the doping concentrations at both sides of the metallurgical junction, are similar in both cases, it is not surprising that W is almost similar and equal to 430 nm. This means that the quasineutral region (in which charge carrier recombination occurs) in the thicker solar cell is larger, resulting in higher recombination. It can be concluded that for the same material properties, thickening the CIGS layer does not necessarily improve the device performance.

5.3 | Bandgap grading

So far, the absorber bandgap was fixed at 1.16 eV, which according to Minoura et al.[1] corresponds to GGI = 0.22. GGI is defined as the compositional ratio of group III elements in the absorber: GGI = [Ga]/([Ga] + [In]). We engineered the absorber bandgap by varying GGI according to energy shift model, described above. Two approaches were taken: (i) constant GGI (0.22) in the first half of absorber thickness (with respect to the front side) and then linear increase of GGI towards the rear side and (ii) linear increase of GGI towards the front side in the first half and then constant GGI in the bottom half of the absorber. In both cases, the maximum value of GGI is 0.9, corresponding to $E_{g\text{-CIGS}}$ = 1.64 eV. Note that this linear profile is merely a simple approach to probe the effect of two opposite bandgap gradings on the cell's performance. Such semilinear profile is already demonstrated in the work of Mansfield et al.[9] More complicated profiles and/or higher (fixed) bandgap can be investigated in future studies. Figure 5 demonstrates the external parameters as functions of front- and rear-side GGI (left-hand side and right-hand side of the dashed line, respectively). The red dashed line corresponds to a constant Ga content of 0.22. It is observed that increasing the Ga content towards the front side of the CIGS layer leads to an increasing trend in V_{OC}. This can be explained by larger quasi-Fermi level splitting due to higher absorber bandgap.[46] Also, there is an optimal value for J_{SC} and η at Front GGI = 0.4. Figure 6A,B provides more information about the reason for this optimum value. According to Figure 6A, which shows the band diagram (in equilibrium) in the top part of the CIGS layer in case of front-side Ga grading, the more the bandgap at the front side of the absorber, the higher is the slope of the conduction band minimum energy. This results in a stronger electric field in that region, increasing the drift of electrons from the front interface

FIGURE 4 A, The external parameters as functions of d_{CIGS}. The bandgap is constant at 1.16 eV. B, Top and bottom: The cross-section of the IBC solar cell with 690 and 1500 nm CIGS thickness, respectively. The colour plot shows the recombination rate under short-circuit conditions. The black curve overlays show the electrostatic potential in equilibrium as a function of depth along the antireflection coating (ARC), CIGS, and transparent conductive oxide (TCO) layers [Colour figure can be viewed at wileyonlinelibrary.com]

FIGURE 5 The external parameters as functions of Ga composition. The red dashed line shows the IBC cell with fixed bandgap. Left-hand side of the dashed line: front-side grading. Right-hand side of the dashed line: rear-side grading [Colour figure can be viewed at wileyonlinelibrary.com]

towards the bulk region (the corresponding *current* has the opposite direction). On the other hand, as can be seen in Figure 6B, an increase in the front-side GGI leads to steeper electron density curve as a function of distance from the front interface. This promotes larger electron diffusion in the direction of the front interface, which counteracts with the drift current. At an optimal value of Front GGI (here, 0.4), the two components of current density outbalance each other, leading to maximum J_{SC} and hence η. This improves the efficiency from 16.73% for the IBC cell with constant bandgap to 17.87% for the IBC cell with optimal bandgap grading.

On the other hand, according to the right-hand side of Figure 5, rear-side Ga grading drastically reduces the cell performance. Although bandgap increase at the bottom half of the

absorber improves V_{OC}, the rest of the external parameters reduce with increasing Rear GGI. The reason is explained by studying the band diagram in the corresponding part of the structure (Figure 6C). We observe the formation of an electron barrier at the CIGS/GZO interface for more Rear GGI. This, in turn, leads to the repulsion of the minority charge carriers from their related contact and, therefore, to an increase in recombination rate in the absorber (Figure 6D). A similar grading in FBC CIGS solar cells enhances the efficiency due to better passivation of the rear contact.[9] We therefore, selected a front-side linear Ga grading with Front GGI = 0.4 as the optimal grading for the rest of simulations. This type of grading can be achieved by introducing a Cu-rich phase instead of the Cu-poor phase in the first stage of the CIGS
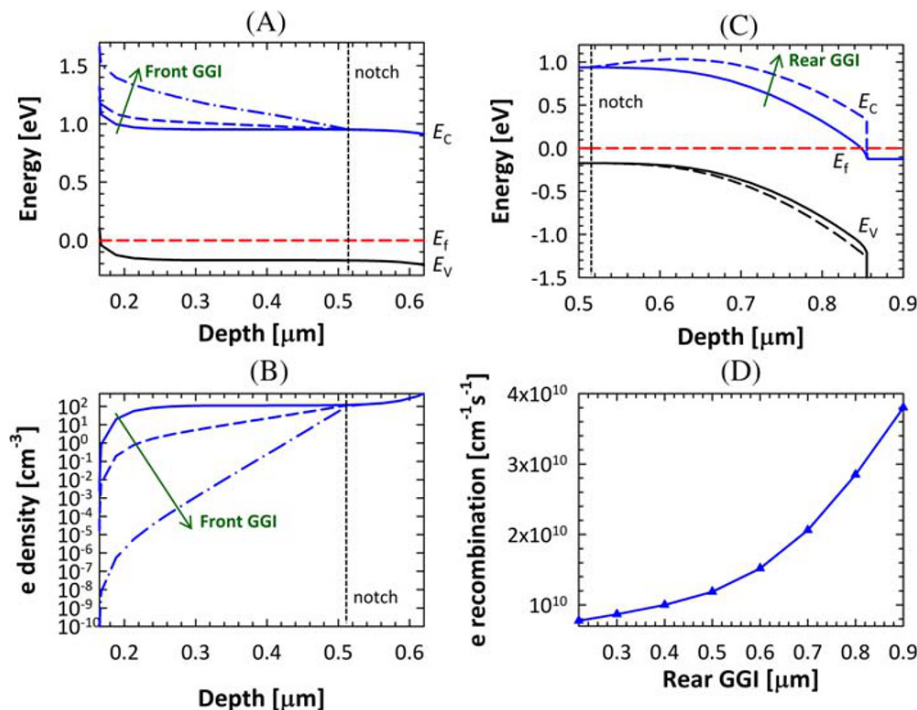
FIGURE 6 A,B, The band diagram and the density of electrons as a function of depth from the front side of the cell in case of front-side grading for Front GGI = 0.22 (blue), 0.4 (black) and 0.9 (red). C, The band diagram in the bottom half of the CIGS layer for Rear GGI = 0.22 (blue) and 0.9 (red). D, The integrated minority carrier recombination rate in the absorber in short-circuit conditions as a function of Rear GGI [Colour figure can be viewed at wileyonlinelibrary.com]

FIGURE 7 The external parameters as functions of (A) *Ratio* = $W_{TCO}/Pitch$ and (B) the bulk donor-type trap density in the absorber [Colour figure can be viewed at wileyonlinelibrary.com]
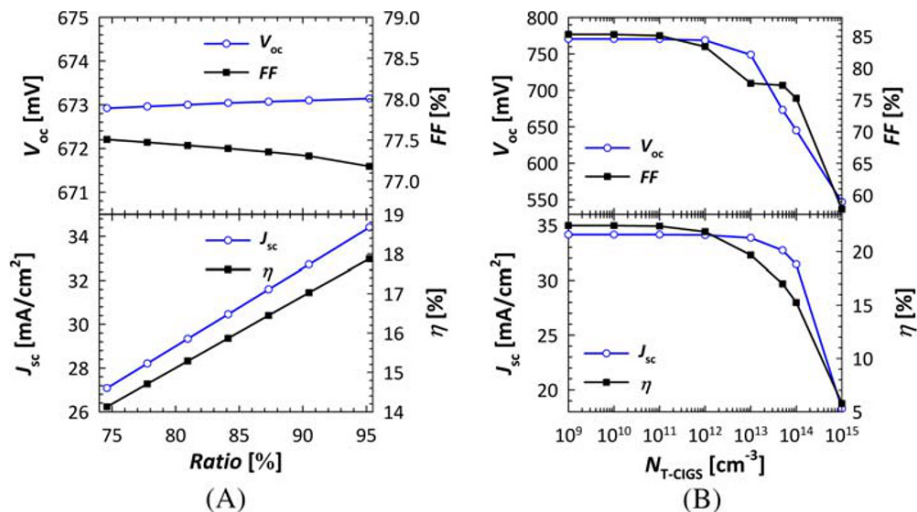
three-stage co-evaporation process, followed by the insertion of group III elements.

It is worth noting that in case of a different absorber thickness, the optimal grading can be different. The results of our thickness-dependent grading optimization are not shown here for brevity.

5.4 | TCO coverage

As discussed above, large values of W_{TCO} lead to less electrical shading and, therefore, to large J_{SC} values. However, Mo contacts wider than what we have considered so far would be less complex to produce. This trade-off is investigated in this section. Here, we define a parameter *Ratio* = $W_{TCO}/Pitch$ and vary it, while keeping *Pitch* and *Gap* constant. In this respect, smaller *Ratio* (smaller W_{TCO}) means larger W_{Mo}. The results are presented in Figure 7A. As expected, stronger electrical shading results from smaller *Ratio* values, thus significantly compromising J_{SC} and η. However, reducing *Ratio* to about 90% still results in η > 17%, which is considerably larger than the efficiency of the FBC reference solar cell. This would allow us to increase W_{Mo} to 2 μm, that is, four times wider than the initial value, and,

therefore, be able to use less complicated and cheaper (lithography) steps for the formation of the h-contact. For this reason, we modified the geometry with a wider Mo contact for further studies (η = 17.02%).

5.5 | Bulk trap density in CIGS

So far, the bulk defect density (N_{T-CIGS}) in the CIGS material was fixed at 5×10^{13} cm^{-3}. However, as the quality of CIGS material can be sensibly better than the one used in our work,[9,11,47] we studied the impact of N_{T-CIGS} on the external parameters (Figure 7B). As expected, a high defect density in the absorber significantly deteriorates the efficiency. On the other hand, improving the material quality, for instance, decreasing N_{T-CIGS} from 5×10^{13} cm^{-3} to 1×10^{13} cm^{-3} can boost the efficiency from 17% to 19.7%. As a result, V_{OC} is increased to values comparable with that of the record CIGS solar cell.[4,5] For a better comparison, the efficiency of the reference FBC solar cell with N_{T-CIGS} = 1×10^{13} cm^{-3} would have been 12.5%. This emphasizes the importance of improving the fabrication process of the CIGS material in the final device performance.

FIGURE 8 Colour plot: electron density, arrows: electric field for the IBC cell (A) with negative fixed charges in the Al$_2$O$_3$ layer and (B) without any fixed charges in equilibrium. The geometrical features of both figures are the same [Colour figure can be viewed at wileyonlinelibrary.com]
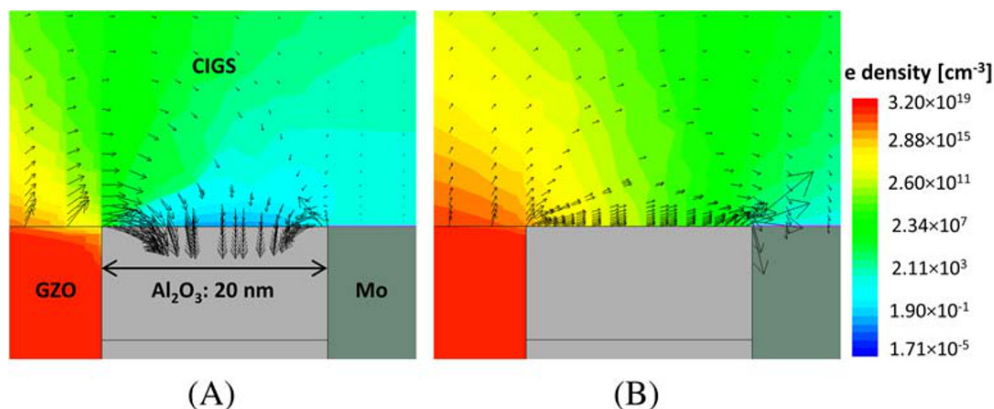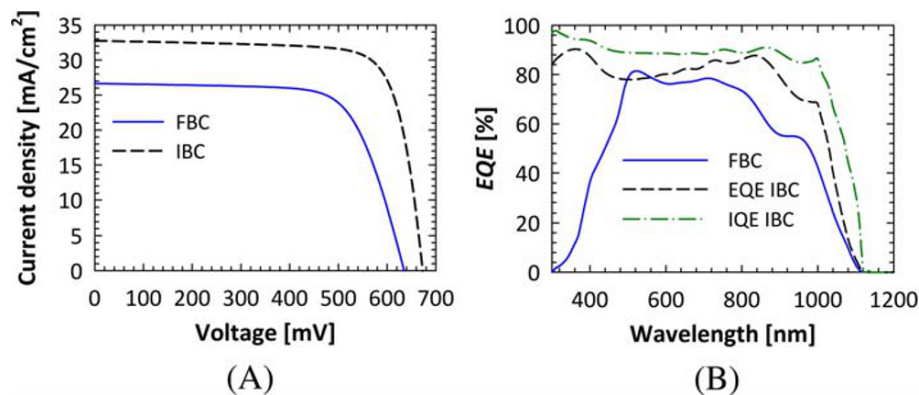
FIGURE 9 Comparison between the reference FBC and the optimized IBC solar cells. (A) Current density versus voltage and (B) EQE and IQE [Colour figure can be viewed at wileyonlinelibrary.com]

5.6 | Gap width

In the previous sections, we briefly mentioned that *Gap* should be as narrow as possible for better charge collection. Indeed, our simulations for different *Gap* widths from 20 nm to 6 μm confirm this. In these models, we kept W_{TCO} and W_{Mo} constant at 28.5 and 2 μm, respectively. N_{T-CIGS} is equal to the reference case of 5×10^{13} cm^{-3}. Increasing *Gap* to values larger than 1 μm mainly affects J_{SC} with a decreasing trend, while other external parameters are nearly unchanged. This is mainly due to the increased hole recombination as a result of larger distance between the generation point and the h-contact. On the other hand, even a gap as narrow as 20 nm is sufficient for high J_{SC} values and avoiding shunts, increasing the efficiency from 17.02% (1-μm wide gap) to 17.34% (20-nm wide gap). From experimental point of view, this is of course more challenging than a 1-μm wide gap. The significant role of the Al_2O_3 layer in the passivation of the contacts is exemplified in Figure 8. There, the electric field vectors are overlaid on the electron density colour plot of the IBC solar cell in equilibrium in two cases: (a) with and (b) without active negative fixed charges in the Al_2O_3 layer. The arrow size shows the intensity of the electric field. The direction of the electric field in case (a) indicates the repulsion of the electrons from the gap area, ensuring the field-effect passivation of the region. This is proved by the colour map of e density in both figures, showing a high density of electrons around the gap and the h-contact in case (b). In case (b), the resulting higher recombination rate degrades all the external parameters and reduces the efficiency from 17.34% to 14.42%.

5.7 | Optimal IBC versus reference FBC

The *J-V* and *EQE* curves of the selected IBC design are compared with the reference FBC solar cell with d_{CIGS} = 673 nm. Note that in this case, the *optimal* design is different from the *ideal* designs studied in Sections 5.5 and 5.6. The former is less experimentally challenging with 90% TCO coverage, 1-μm *Gap* and the reference trap density in the absorber material. The improvement in all the external parameters is evident in Figure 9. The difference between *EQE* and internal quantum efficiency (*IQE*) curves of the IBC solar cell in Figure 9B is an

indication of incomplete charge carrier collection that yet needs to be addressed. Nonetheless, the difference between the *EQE* spectra of the two structures is substantial. It should also be noted that unlike the optically optimized IBC structure in our previous work,[27] the flat interface design of the IBC solar cell in this work results in lower values of *IQE*. Better light in-coupling can be achieved by a more effective ARC.[14,27]

6 | CONCLUSION

We proposed and optimized an IBC structure for boosting the efficiency of a CIGS solar cell with a submicron thickness (precisely, 673 nm). In this configuration, the parasitic absorption of the front layers and the optical shading of the front-contact are prevented. We used 2-D opto-electrical simulations in TCAD Sentaurus environment to accurately model such solar cell architecture. The study of the band diagram shows a good electrical passivation at the front side of the absorber due to the negative charges in the Al_2O_3 layer. Also, the band bending in the CIGS/e-contact interface area is an indication of an effective electron selective contact.

The study of the TCO width shows that the wider the TCO, the less the electrical shading is and the higher the efficiency is. Increasing the absorber thickness, while keeping the electronic features constant, results in higher charge carrier recombination in the absorber bulk and hence worse performance. This is because of a larger quasineutral region with respect to the total bulk area in thicker absorbers.

We showed that a bandgap grading with higher bandgap at the front side of the CIGS layer improves the efficiency by 1.1 abs.%, compared with the case with constant bandgap. However, because of the trade-off between the resulting drift and diffusion currents, there is an optimum grading for maximum efficiency. Note that the optimal grading can vary with the absorber thickness.

Our studies on the geometrical properties of the e- and h-contacts show that although a wider TCO and a narrower Mo (less than 1 μm) are more favourable for higher efficiencies, this complicates the fabrication of the Mo layer. This can be addressed by reducing the TCO width (hence, widening Mo) from 30 to 28.5 μm, at the expense of about 0.8 abs.% loss in efficiency. In this case, compared with 11.9% for the reference FBC solar cell, the IBC structure shows a conversion efficiency of 17%.

Since the quality of our simulated absorber from defect density point of view is lower than the state-of-the-art CIGS absorber material, we studied the effect of defect density on the cell performance. We observed that by reducing the bulk defect density from 5×10^{13} cm^{-3} to 1×10^{13} cm^{-3}, the efficiency can be improved to 19.7%.

The sensitivity of the performance on the gap width was checked by changing *Gap* from 20 nm to 6 μm. The higher recombination with a wider gap reduces the current density. On the other hand, the performance improves as *Gap* is shrunk. The electric field map shows that the presence of negative fixed charges in the Al$_2$O$_3$ layer ensures the electrical passivation and low recombination at small *Gap* values.

We showed how an IBC structure with optimal bandgap grading and high absorber quality can help us achieve high efficiencies with submicron CIGS layers. Indeed, better optical performance is still possible by, for example, high aspect ratio ARC.[14] Although the proposed structure needs to answer many fabrication challenges, including potentially costly patterning steps, it can pave the way towards high-efficiency thin-film CIGS solar cells and their deployment in three- and four-terminal tandem devices.

ACKNOWLEDGEMENT

CONFLICT OF INTEREST

The authors report no potential conflict of interest.

ORCID

Nasim Rezaei https://orcid.org/0000-0003-1244-3717
Paul Procel https://orcid.org/0000-0003-4997-3551
Olindo Isabella https://orcid.org/0000-0001-7673-0163

REFERENCES

1. Minoura S, Maekawa T, Kodera K, Nakane A, Niki S, Fujiwara H. Optical constants of Cu (In, Ga)Se$_2$ for arbitrary Cu and Ga compositions. *J Appl Phys*. 2015;117(19):195703.
2. van Lare C, Yin G, Polman A, Schmid M. Light coupling and trapping in ultrathin Cu (In, Ga) Se$_2$ solar cells using dielectric scattering patterns. *ACS Nano*. 2015;9(10):9603-9613.
3. Poncelet O, Kotipalli R, Vermang B, Macleod A, Francis LA, Flandre D. Optimisation of rear reflectance in ultra-thin CIGS solar cells towards > 20% efficiency. *Sol. Energy*. 2017;146:443-452.
4. Green MA, Dunlop ED, Levi DH, Hohl-Ebinger J, Yoshita M, Ho-Baillie AWY. Solar cell efficiency tables (version 54). *Prog Photovoltaics Res Appl*. 2019;27(7):565-575.
5. Nakamura M, Yamaguchi K, Kimoto Y, Yasaki Y, Kato T, Sugimoto H. Cd-Free Cu (In,Ga)(Se,S) 2 Thin-Film Solar Cell With Record Efficiency of 23.35%. *IEEE J Photovoltaics*. 2019;9(6):1863-1867.
6. Shockley W, Queisser HJ. Detailed balance limit of efficiency of p-n junction solar cells. *J Appl Phys*. 1961;32(3):510-519.
7. Topic M, Geisthardt RM, Sites JR. Performance limits and status of single-junction solar cells with emphasis on CIGS. *IEEE J. Photovoltaics*. 2015;5(1):360-365.
8. Suresh S, de Wild J, Kohl T, et al. A study to improve light confinement and rear-surface passivation in a thin-Cu (In, Ga)Se$_2$ solar cell. *Thin Solid Films*. 2019;669:399-403.
9. Mansfield LM, Kanevce A, Harvey SP, et al. Efficiency increased to 15.2% for ultra-thin Cu (In,Ga)Se$_2$ solar cells. *Prog Photovoltaics Res Appl*. 2018;26(11):949-954.
10. Naghavi N, Mollica F, Goffard J, et al. Ultrathin Cu (In,Ga)Se$_2$ based solar cells. *Thin Solid Films*. 2017;633:55-60.
11. Ramanathan K, Noufi R, To B, et al. Processing and properties of sub-micron CIGS solar cells. *Conf. Rec. 2006 IEEE 4th World Conf. Photovolt. Energy Conversion*, WCPEC-4. 2006;(1):380-383.
12. Kovacic M, Krc J, Lipovsek B, et al. Light management design in ultra-thin chalcopyrite photovoltaic devices by employing optical modelling. *Sol. Energy Mater. Sol. Cells*. 2019;200:109933.
13. Yin G, Manley P, Schmid M. Light trapping in ultrathin CuIn1-xGaxSe2 solar cells by dielectric nanoparticles. *Sol Energy*. 2018;163:443-452.
14. Rezaei N, Isabella O, Vroon Z, Zeman M. Optical optimization of a multi-layer wideband anti-reflection coating using porous MgF2 for sub-micron-thick CIGS solar cells. *Sol. Energy*. 2019;177:59-67.
15. Kotipalli R, Poncelet O, Li G, et al. Addressing the impact of rear surface passivation mechanisms on ultra-thin Cu (In,Ga)Se$_2$ solar cell performances using SCAPS 1-D model. *Sol. Energy*. 2017;157:603-613.
16. Mollica, F., Goffard J, Jubault M, Donsanti F, Collin S, Cattoni A, Lombez L, Naghavi N. Comparative study of patterned TiO$_2$ and Al$_2$O$_3$ layers as passivated back-contact for ultra-thin Cu(In, Ga)Se$_2$ solar cells. in *Photovoltaic Specialists Conference (PVSC), 2016 IEEE 43rd* 6–10 (IEEE, 2016).
17. Friedlmeier TM, Jackson P, Bauer A, et al. High-efficiency Cu(In,Ga)Se$_2$ solar cells. *Thin Solid Films*. 2017;633:13-17.
18. Siebentritt S. What limits the efficiency of chalcopyrite solar cells? *Sol Energy Mater Sol Cells*. 2011;95(6):1471-1476.
19. Hara T, Maekawa T, Minoura S, Sago Y, Niki S, Fujiwara H. Quantitative assessment of optical gain and loss in submicron-textured CuIn$_{1-x}$Ga$_x$Se$_2$ solar cells fabricated by three-stage coevaporation. *Phys Rev Appl*. 2014;2(3):34012.
20. Reinhard P, Chirila A, Blosch P, et al. Review of progress toward 20% efficiency flexible CIGS solar cells and manufacturing issues of solar modules. *IEEE J Photovoltaics*. 2013;3(1):572-580.
21. Yang G, Guo P, Procel P, et al. High-efficiency black IBC c-Si solar cells with poly-Si as carrier-selective passivating contacts. *Sol Energy Mater sol Cells*. 2018;186:9-13.
22. Wagner P, Stang JC, Mews M, Morales-Vilches AB, Stannowski B, Stegemann B, Korte L Interdigitated back contact silicon heterojunction solar cells: towards an industrially applicable structuring method. in *AIP Conference Proceedings* **1999**, 060001 (2018).
23. Savin H, Repo P, von Gastrow G, et al. Black silicon solar cells with interdigitated back-contacts achieve 22.1% efficiency. *Nat Nanotechnol*. 2015;10(7):624-628.
24. Franklin E, Fong K, McIntosh K, et al. Design, fabrication and characterisation of a 24.4% efficient interdigitated back contact solar cell. *Prog Photovoltaics Res Appl*. 2016;24:411-427.
25. Nakamura J, Asano N, Hieda T, Okamoto C, Katayama H, Nakamura K. Development of heterojunction back contact Si solar cells. *IEEE J. Photovoltaics*. 2014;4(6):1491-1495.
26. Haase F, Hollemann C, Schäfer S, et al. Laser contact openings for local poly-Si-metal contacts enabling 26.1%-efficient POLO-IBC solar cells. *Sol Energy Mater Sol Cell*. 2018;186:184-193.
27. Rezaei N, Isabella O, Procel P, Vroon Z, Zeman M. Optical study of back-contacted CIGS solar cells. *Opt Express*. 2019;27(8):A269-A279.
28. Smith DD, Cousins PJ, Masad A, et al. SunPower's Maxeon Gen III solar cell: High efficiency and energy yield. *Conf. Rec. IEEE Photovolt. Spec. Conf.* 908–913 (2013). doi:https://doi.org/10.1109/PVSC.2013.6744291
29. Masuko K, Shigematsu M, Hashiguchi T, et al. Achievement of more than 25% conversion efficiency with crystalline silicon heterojunction solar cell. *IEEE J. Photovoltaics*. 2014;4(6):1433-1435.

30. Yoshikawa K, Kawasaki H, Yoshida W, et al. Silicon heterojunction solar cell with interdigitated back contacts for a photoconversion efficiency over 26%. *Nat Energy*. 2017;2(5):17032.

31. Tomasi A, Paviet-Salomon B, Jeangros Q, et al. Simple processing of back-contacted silicon heterojunction solar cells using selective-area crystalline growth. *Nat Energy*. 2017;2(5):17062.

32. Sivaramakrishnan Radhakrishnan H, Uddin MDG, Xu M, et al. A novel silicon heterojunction IBC process flow using partial etching of doped a-Si:H to switch from hole contact to electron contact in situ with efficiencies close to 23%. *Prog Photovoltaics Res Appl*. 2019;27(11):959-970.

33. Takagishi H, Noge H, Saito K, Kondo M. Fabrication of interdigitated back-contact silicon heterojunction solar cells on a 53-μm-thick crystalline silicon substrate by using the optimized inkjet printing method for etching mask formation. *Jpn J Appl Phys*. 2017;56(4):040308.

34. Procel P, Yang G, Isabella O, Zeman M. Theoretical evaluation of contact stack for high efficiency IBC-SHJ solar cells. *Sol. Energy Mater. Sol. Cells*. 2018;186:66-77.

35. Frisk C, Platzer-Björkman C, Olsson J, et al. Optimizing Ga-profiles for highly efficient Cu(In, Ga)Se$_2$ thin film solar cells in simple and complex defect models. *J Phys D Appl Phys*. 2014;47(48):485104.

36. Fujiwara H, Kondo M. Effects of carrier concentration on the dielectric function of ZnO:Ga and In$_2$O$_3$:Sn studied by spectroscopic ellipsometry: analysis of free-carrier and band-edge absorption. *Phys Rev B - Condens Matter Mater Phys*. 2005;71:1-10.

37. Snyder PG, Woollam JA, Alterovitz SA, Johs B. Modeling Al$_x$Ga$_{1-x}$As optical constants as functions of composition. *J Appl Phys*. 1990;68(11):5925-5926.

38. Lundberg O, Bodegård M, Malmström J, Stolt L. Influence of the Cu(In,Ga)Se$_2$ thickness and Ga grading on solar cell performance. *Prog. Photovoltaics Res Appl*. 2003;11:77-88.

39. Onwudinanti C, Vismara R, Isabella O, Grenet L, Emieux F, Zeman M. Advanced light management based on periodic textures for Cu(In,Ga)Se$_2$ thin-film solar cells. *Opt Express*. 2016;24(6):A693-A707.

40. Dingemans G, Kessels WMM. Status and prospects of Al$_2$O$_3$-based surface passivation schemes for silicon solar cells. *J Vac Sci Technol A Vacuum, Surfaces, Film*. 2012;30, 040802.

41. Dodge MJ. Refractive properties of magnesium fluoride. *Appl Optics*. 1984;23(12):1980-1985.

42. Rezaei N, Isabella O, Vroon Z, Zeman M. Quenching Mo optical losses in CIGS solar cells by a point contacted dual-layer dielectric spacer: a 3-D optical study. *Opt Express*. 2018;26(2):A39-A53.

43. Kotipalli R, Vermang B, Joel J, Rajkumar R, Edoff M, Flandre D. Investigating the electronic properties of Al$_2$O$_3$/Cu(In,Ga)Se$_2$ interface. *AIP Adv*. 2015;5(10):107101.

44. Isabella O, Sai H, Kondo M, Zeman M. Full-wave optoelectrical modeling of optimized flattened light-scattering substrate for high efficiency thin-film silicon solar cells. *Prog Photovoltaics Res Appl*. 2014;22(6):671-689.

45. Hermle M, Granek F, Schultz-Wittmann O & Glunz SW. Shading effects in back-junction back-contacted silicon solar cells. *Conf. Rec. IEEE Photovolt. Spec. Conf*. 10–13 (2008). doi:https://doi.org/10.1109/PVSC.2008.4922761

46. Smets A, Jäger K, Isabella O, van Swaaij R, Zeman M. *Solar Energy: The Physics and Engineering of Photovoltaic Conversion, Technologies and Systems*. UIT Cambridge Limited; 2016.

47. Kim K, Park H, Kim WK, Hanket GM, Shafarman WN. Effect of reduced Cu (InGa)(SeS)$_2$ thickness using three-step H2Se/Ar/H2S reaction of Cu-In-Ga metal precursor. *IEEE J Photovoltaics*. 2013;3(1):446-450.